SCIENTIFIC REPORTS

OPEN

Brain hubs in lesion models: Predicting functional network topology with lesion patterns in patients

Received: 11 July 2017
Accepted: 2 December 2017
Published: xx xx xxxx
Published online: 20 December 2017

Binke Yuan , Yuxing Fang , Zaizhu Han , Luping Song , Yong He & Yanchao Bi

H

multivariate support vector regression analysis on brain structural and resting-state functional imaging

P

I

O

e human brain comprises highly interconnected units on multiple scales. At the macroscale level, the functional connectivity between regions can be measured as the temporal correlation of time courses of blood oxygen level-dependent uctuations of functional magnetic resonance imaging[1]. e human whole-brain functional network can be constructed based on inter-regional functional connectivity and its topological properties can be studied with graph theory approaches[2,3]. One of the major ndings in such "connectomic" literature in the past decade is the identi cation of a set of brain regions that are thought to play more important roles in the network communication than others, which tend to be implicated in various types of degenerative disease[4,5]. ese regions are o en considered the brain "hubs"[6].

e "importance" of a brain region in the functional network structure has been considered from di erent aspects. One of the most common ways is to simply look at the number and/or strength of functional connections a region has (i.e., degree centrality). is approach has consistently identi ed the posterior cingulate cortex/precuneus (PCC/PCu), the medial prefrontal cortex (mPFC) and the inferior parietal gyrus as "hubs"[7–9]. Other methods have been proposed to de ne hub regions that take into consideration other topological aspects of the network such as modular structure[10–13], considering regions that are the most important in linking di erent functional modules as connector hubs. ese connector hubs, de ned on the basis of "participation coe cient" (PC)[14], i.e., the proportion of the number of a region's inter-module connections to its total connections, mainly distributed in the anterior insula, the bilateral middle frontal gyrus (MFG), the bilateral precentral gyrus, the dorsal mPFC, and the superior parietal cortex.

A critical alternative approach to determining the importance of a region in network communication is to examine how much the network properties are altered if a given region is damaged. In patients with brain lesions, Gratton *et al.*[11] found that the mean lesion severity (the nodal lesion percentages scaled by the region's centrality measure in the healthy group) of regions with high PCs, not those with high within-module degree (WMD)[14], was signi cantly correlated with the modularity property of the patient's functional network. Such results o er compelling evidence that regions with higher PCs are more indispensable in maintaining a functional network's

[1]National Key Laboratory of Cognitive Neuroscience and Learning and IDG/McGovern Institute for Brain Research, Beijing Normal Univer i
equally to this work. Correspondence and requests for materials should be addressed to Y.B. (email: ybi@bnu.edu.cn)

Figure 1. Overview of the methods to detect lesion hubs. (**a**) First, lesion pattern (i.e., lesion percentages of nodes) and network topology of the binary functional network were calculated for each of the 96 patients. en, a lesion model using SVR was trained with lesion patterns of 95 patients as features, and network topological measures as training labels. Next, the trained model were used to predict the network topology of the test patient with his or her lesion pattern. A nested LOOCV was applied and the prediction accuracy of each lesion model was evaluated by calculating the Pearson correlation coe cient between the predicted labels and real labels. A er 1000 permutation tests, the model signi cance was calculated. For the lesion model which could be signi cantly predicted by lesion patterns, features with signi cant weights were extracted, and considered as "lesion hubs". (**b**) e averaged functional network of the 144 healthy participants was used to construct a healthy connectome, on which modularity analyses were performed and nodal metrics were calculated.

modularity and, hence, are more important hubs. Nevertheless, many important issues remain to be addressed. First, brain lesion is neither comparable nor independent across regions[15,16]. e distribution of brain lesions is complexly constrained by vascular properties and should be understood as a high-dimensional multivariate pattern, which cannot be adequately addressed by the univariate or multiple linear regression approaches. Second, this study did not test the impact of lesion for speci c regions. Furthermore, the changing directions of network topology a er lesions have been shown to be complex[17], and lesions of di erent regions might lead to opposite direction of changes on the small-worldness – the balance between the integration and segregation – of the remaining network[18,19]. For instance, Sporns *et al.*[18] showed that simulated lesions in connector hubs increase the distance among modules and led to increased clustering coe cient and small-worldness, while simulated lesions in within-module hubs decrease these measures. Given that simulation lesion studies[10,20,21] relies on speci c assumptions about the mechanisms of attack, which does not necessarily re ect actual brain lesion patterns, studies based on real brain damage data that employ multi-variate approaches are needed to understand how lesion encompassing various brain regions a ect functional network topology.

We applied a multivariate support vector regression (SVR) approach to evaluate the relationship between brain lesion patterns (i.e., the pattern of lesion extent across various cerebrum nodes) and whole-brain functional network topological properties in 96 patients with brain damage (Fig. 1). In contrast to univariate approaches, where each region is examined separately (e.g., linear regression), SVR involves a linear regression analysis in a high-dimensional feature space (here, lesion percentage in each region as features) to make continuous measurement predictions[22–24]. e SVR model yields weights for each region, indexing the extent to which the region's lesion contributes to the prediction of di erent topological properties[15,16]. Regions with higher predictive weights indicate that their damage would lead to greater changes of the functional network and are more indispensable.

ese regions are thus considered "lesion hubs". Finally, we compared these lesion hubs to those hubs conventionally de ned by graph attributes in the functional network in a healthy population to understand the relationship between these two perspectives of delineating brain network properties.

Results

Ninety-six patients (19 females, mean age SD = 44.56 years 13.21, range 19–74 years) with focal brain damages in sub-acute and chronic phase were analyzed (see Table S1 for details). e Craddock parcellation[25]

containing 180 cerebrum nodes were adopted and for each patient the lesion percentage in each node was calculated (see Figure S1 for lesion overlap map). All but two nodes have at least one patient with damaged voxels. e lesion percentages of the 178 nodes were used as features for the linear SVR[24] analysis to predict functional network topological properties.

L For functional network topological properties, we rst considered small-worldness (sigma), a composite measure about the extent of optimal balance of functional integration and segregation, then in the subsequent analyses looked at network global e ciency (network gE) and network local e ciency (network locE) separately to understand the direction of lesion-induced changes in the context of a ecting the small-worldness. We calculated these topological properties in a single threshold (sparsity, $s = 0.15$) in the main analyses and validated the results by calculating the cumulative topological properties in the full range of network sparsity using the area under curve (AUC) method[26]. Leave-one-out-cross-validation (LOOCV) were used to calculate the prediction accuracy (the Pearson correlation coe cient between the predicted and actual labels) and signi cance level was computed based on 1000 permutation tests[23]. Note that we also examined models where the total lesion volume was included as an additional predictor. e rationale was lesion pattern might be a ected by total lesion volume, and if it was the lesion volume that was the actual signi cant predictor for network topology, rather than the lesion pattern (speci c lesion distribution), in the SVR model its contribution should be signi cant and the lesion regional features would not.

Permutation test found that the whole-brain lesion pattern, i.e., the distribution pattern of the lesion across the 178 nodes, predicted functional network small-world sigma with signi cantly above-chance accuracies ($r = 0.223$, Pone-tailed $= 0.025$). In ow-up analyses to test the direction (integration or segregation) that contributes to the sigma changes, we found that the whole-brain lesion pattern signi cantly predicted network gE ($r = 0.269$, Pone-tailed $= 0.015$) and network locE ($r = 0.220$, Pone-tailed $= 0.041$). Figure S2 showed the scatter plots of the actual network topological property values and the predicted values using these three signi cant lesion models and the corresponding linear regression lines. Without the total lesion volume as a feature, signi cant above-chance accuracies were observed for small-world sigma ($r = 0.225$, Pone-tailed $= 0.024$) and network gE ($r = 0.268$, Pone-tailed $= 0.019$), with a positive trend for network locE ($r = 0.183$, Pone-tailed $= 0.055$). at is, the performances of these lesion models were minimally a ected a er adding the total lesion volume as one additional feature.

A split-half analysis was also conducted to validate the e ectiveness of the lesion models. We randomly divided the patients into two subgroups and then performed SVR prediction in each subgroup. e results were relatively reliable: For small-world sigma, the signi cant prediction was observed in subgroup2 (subgroup1: $r = 0.185$, Pone-tailed $= 0.091$; subgroup2: $r = 0.425$, Pone-tailed $= 0.013$). Signi cant predictions were observed in both subgroups for network gE (subgroup1: $r = 0.383$, Pone-tailed $= 0.006$; subgroup2: $r = 0.402$, Pone-tailed $= 0.007$), and network locE (subgroup1: $r = 0.348$, Pone-tailed $= 0.018$; subgroup2: $r = 0.392$, Pone-tailed $= 0.013$).

L **R** e predictive weight of each feature was obtained by training a SVR model using all patients. e unthresholded maps of the feature weights in the three regression models are shown in Fig. 2 (rst row). Features with signi cantly above-chance ($P < 0.05$, permutation test, two-tailed) weights were extracted (Fig. 2, second row). e weight of the total lesion volume did not reach signi cant in any models. As shown in Fig. 2 and Table 1, the following regions showed signi cantly negative weights in the prediction models for network locE and sigma and signi cantly positive weights in the prediction model for network gE: the le MFG, the bilateral superior frontal gyrus, and the orbital frontal pole. Clusters in the right superior temporal gyrus (STG; extending into the supramarginal gyrus), the superior portion of the le temporal pole (sTP), the bilateral superior frontal gyrus (SFG), the bilateral mPFC and the bilateral insula also showed this pattern, although their e ects did not reach signi cance in all three models.

ere were also regions showing the opposite pattern, with positive weights for the lesion models of network locE and sigma and/or negative weights for network gE: e pars opercularis and pars triangularis of the right inferior frontal gyrus (IFG oper and IFG tri) had signi cantly positive weights for network locE and sigma; e le anterior middle temporal gyrus (aMTG, extending to the middle part of MTG) had signi cantly positive weights for network locE; e right hippocampus had signi cantly negative weight for network gE; e bilateral paracingulate cortex (paraCC), the bilateral dorsal anterior cingulate gyrus (dACC) and the le precentral gyrus had signi cantly positive weights for sigma. e feature of the total lesion volume did not show signi cant weight in any lesion model.

To incorporate lesion hubs obtained from the three graph measures, we plotted all signi cant regions from these models in Fig. 3a, with two colors corresponding to the two classes, i.e., those whose lesion induced more integrated/global processing (reduced network locE or sigma and/or increased network gE), and those whose lesion induced more segregated/local processing (increased network locE or sigma and/or reduced network locE).

R We constructed a healthy functional network using the same Craddock atlas ($n =$

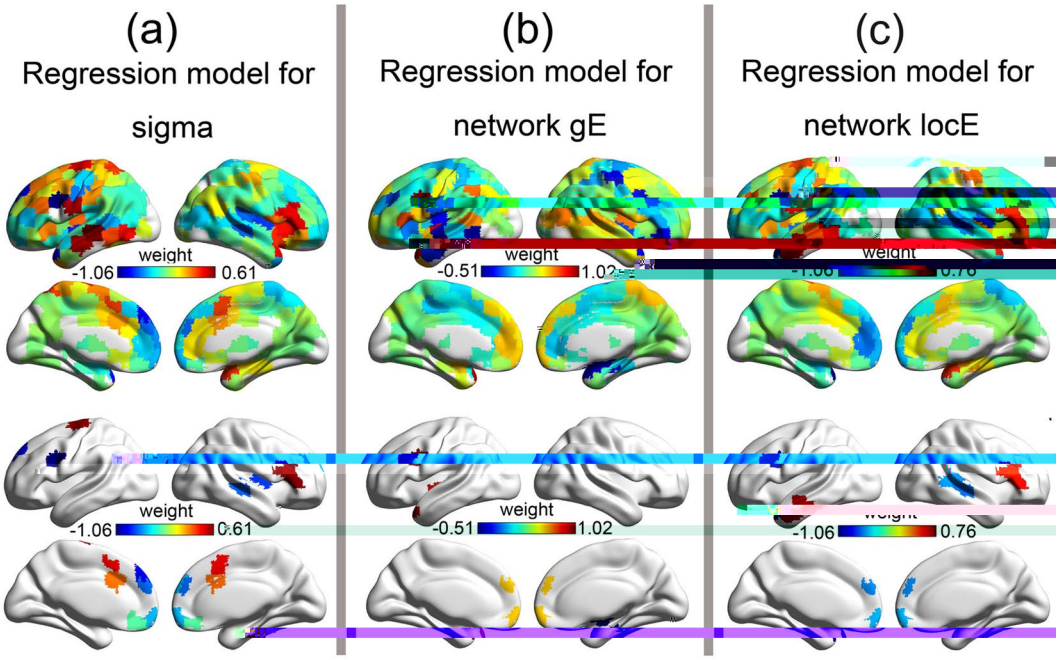

Figure 2. Feature weights and lesion hubs in signi cant lesion models. e rst row shows the distributions of feature weights in the three signi cant lesion models. e second row shows the lesion hubs with signi cant feature weights ($P < 0.05$, two-tailed, permutation test) in each of the three signi cant lesion models. Cold colors represent negative weights and warm colors indicate positive weights.

identi ed (Fig. S3a and b). We then chose a representative sparsity, $s = 0.15$ to check the modular assignment (Fig. S3c and d) and calculated the nodal properties. e lesion hubs were distributed in DMN, FPN and SSN in the healthy network (Table 1).

e hub distributions in the healthy network were analyzed based on three nodal metrics: participant coe - cient (PC) and within-module degree (WMD), re ecting nodal roles in connecting di erent modules and within each module, respectively, and nodal gE, measuring global information communication e ciency. e distributions for each of the three nodal metrics are shown in Figs S3(e,f,g) and S4, and the regions showing relatively high nodal properties ($PC > 0.3$, $WMD > 0$, nodal $gE_{Z\text{-score}} > 0$) are in accordance with ndings in the literature.

e two classes of lesion hubs tended to exhibit high nodal metrics in the healthy connectome. As shown in Table 1 and Fig. 3b, lesion hubs that are of the "integration e ect" class in the le MFG and the right STG, and lesion hubs of the "segregation e ect" class in the right IFG tri and IFG oper, were connectors with high nodal PC (> 0.3). e other lesion hubs belonging to either class were provincial hubs with high nodal WMD (> 0): e "integration e ect" lesion hubs in the bilateral SFG, the bilateral FP orb, the le sTP, the bilateral mPFC and the bilateral insula, and the "segregation e ect" lesion hubs in the le aMTG, the bilateral dACC, the bilateral paraCC and the le precentral gyrus. All lesion hubs (except the right hippocampus) also showed high nodal gE (Z-score > 0).

Intriguingly, there are also regions with high nodal metrics in the healthy connectome that did not show signi cantly weights in the lesion models: the PCC/PCu, the lateral parietal cortex, the dorsolateral prefrontal cortex (DLPFC).

R A series of validation analyses were performed to examine the robustness of the main results by using di erent network construction procedures (sparsity thresholds; head motion treatment; global signal removal; parcellation scheme) or participant selection methods (right-handed stroke patients, only male patients). e prediction accuracies of the validation analyses are summarized in Table S3. Details are described below.

e e ects of the network sparsity thresholds. To consider the results across a broad sparsity range, we calculated the cumulative values of the network metrics by using the AUC[26] for each network metric across the sparsities of 0.13–0.47 (step 0.01, see Method for the identi cation method of the sparsity range), to avoid potential bias in selecting a speci c sparsity. Using such AUC metrics as labels, the predictive accuracies for the three lesion models remained signi cant (sigma: $r = 0.29$, $P_{one\text{-}tailed} = 0.013$, network locE: $r = 0.317$, $P_{one\text{-}tailed} = 0.007$, and network gE: $r = 0.287$, $P_{one\text{-}tailed} = 0.012$). e brain regions with signi cant weights in these three signi cant lesion models were nearly identical to those in the main results (Fig. S5).

Motion scrubbing. A er the "scrubbing" procedure was performed on the preprocessed images to further deal with head motion, one patient was excluded because the number of remaining volumes was fewer than

50. Signi cant prediction were observed for sigma ($r = 0.241$, *Pone-tailed* $= 0.033$), network locE ($r = 0.244$, *Pone-tailed* $= 0.019$) and network gE ($r = 0.246$, *Pone-tailed* $= 0.024$) were still signi cant. In the three signi cant lesion models, the distributions of the brain regions with signi cant feature weights were largely consistent with the main results (Fig. S6).

e e ect of global signal regression (GSR). We perform GSR to reduce the motion-induced noises[29] in the main analysis. When the global signals were not removed, the predictive accuracy was signi cant in the lesion model for network locE ($r = 0.249$, *Pone-tailed* $= 0.019$), and not for network gE ($r = 0.168$, *Pone-tailed* $= 0.067$) or sigma ($r = 0.093$, *Pone-tailed* $= 0.136$). For network locE, the same lesion hubs to those in the main results were obtained: the le sTP and the right STG with negative weights and the le aMTG with positive weight.

e e ect of brain parcellation. We repeated the whole analyses using another brain parcellation – Brainnetome Atlas[30] (246 nodes) – to investigate whether the results are a ected by the choice of parcellation scheme. We chose this atlas because its parcellation was done on the basis of structural connectivity and had comparable number of regions with the Craddock 200 atlas. We also considered a third atlas, Craddock atlas with 1000 parcellations[25], which contained much ner parcellations and could help to re ne the main ndings. When using the Brainnetome atlas, all three lesion models were still signi cant, with better performance than the main results: for sigma, $r = 0.449$, *Pone-tailed* < 0.001; for network gE, $r = 0.454$, *Pone-tailed* < 0.001; for network locE, $r = 0.387$, *Pone-tailed* $= 0.002$. Features with signi cant weights that covered the same brain regions (e.g., the le MFG, the le TP, the right IFG and the le precentral gyrus) and showing the same type of lesion e ects as those in the main results were observed (Fig. S7). While other lesion hubs detected using Craddock 200, including the le mPFC, the le FP and the right insula and the bilateral dACC, did not reach signi cance in the model using the Brainnetome Atlas, they nonetheless had relative greater weights than the average (top 50%). When using the "Craddock 1000 atlas"[25], lesion pattern still predicted functional network small-world sigma (in sparsity threshold, $s = 0.01$, an arbitrary threshold to ensure sparse and fully-connected networks, Table S3) with above-chance accuracies ($r = 0.188$, 1000 permutation tests *P*one-tailed $= 0.045$), as well as network gE ($r = 0.267$, *P*one-tailed $= 0.016$) and network locE ($r = 0.319$, *P*one-tailed $= 0.004$). e signi cant contributing features (brain regions, Fig. S8) aligned more di erently from the other two atlases (Craddock 200 and Brainnetome). e di erences for the signi cant predictor brain regions across atlases might be because using a ner brain

parcellation with too many features (1000 partitions), correlations among features are much higher (the per-

with both lesion-hub classes containing regions with high PC and also regions with high WMD. ere were also hubs in the healthy connectome that were not observed as lesion hubs.

Di erent from previous studies about the e ects of lesion in functional network topology using univariate methods[11,13,20,21] (see a review by Aerts *et al*. ref.[17]), we used a more appropriate (multivariate) approach for real brain damage data that takes into consideration of the complex interaction of lesion patterns across brain regions. We established that aspects of the integration and segregation properties of functional network topological characteristics can be predicted from the pattern of brain lesions, including small-worldness (the balance between integration and segregation), network global (relative integration) and local e ciency (relative segregation). Such e ects of lesion distribution patterns were not explained by the overall extent of lesion because the total lesion volume was not a signi cant predictor for topology in the SVR model. at is, it is not the sheer size of the lesion but the distribution pattern of the lesion that matters for the network's integrity.

e multivariate lesion models also provide the speci c manner in which their lesion changes the functional network topology (i.e., the feature weights and sign). Our results revealed two distinct classes of lesion-hubs, whose lesions cause the whole functional network to be either signi cantly more integrated (lower network locE or sigma and/or higher network gE) or signi cantly more segregated (higher network locE or sigma and/or lower network gE). All lesion-hub regions (except the right hippocampus) in these two classes show relatively high centrality measures in healthy functional connectome, indicating the overall correspondence between di erent approaches in identifying regional importance in the network topology. e manner of correspondence, however, is rather complex, with both classes of lesion hubs containing both regions with high PC (i.e., connectors between di erent systems) and regions with high WMD (i.e., provincial hubs within speci c systems). Below, we discuss these two-class lesion hubs in the context of their status in the healthy functional connectome in greater details.

L Some of this type of lesion hubs have high WMD in healthy connectome: the bilateral SFG, the bilateral FP orb, the le sTP, the bilateral mPFC and the bilateral insula. ese regions have been consistently identi ed as hub regions in previous studies using the degree-based approaches, with all regions except the insula belonging to the so-called DMN system, which is more active during rest and is deactivated during explicit tasks[7,8,10,12,34,35]. at is, these regions have the greatest number and/or strength of functional connections with other regions in the healthy system. Physiological studies have shown that regions with a high degree, including this type of lesion hubs, tend to have high biological cost, with high rates of cerebral blood ow, aerobic glycolysis and oxidative glucose metabolism[9,36–38]. Also, their changes are strongly associated with various types of neurological disorders[39,40]. e insula was identi ed as a provincial hub with high WMD and gE in the current study, and previous studies have regarded it as a connector with high PC[12] or a rich-club region[41] and participating a wide range of cognitive functions[42,43]. Our ndings provide direct evidence for the necessity role of these regions in the organization of the whole-brain functional network.

Other lesion-hubs that have the "integrated-topology e ect", the le MFG and the right STG, have high nodal PC in the healthy connectome, meaning that they have particularly more and/or stronger connections across di erent modules and are thus likely to integrate information from di erent functional systems[42,43]. e le MFG connects FPN and SSN, the right STG connects DMN and SSN (Fig. S2). e MFG node also contained large part (44%) of the le inferior frontal junction, a critical node for cognitive control[44]. Complementing previous studies using univariate lesion or simulated-lesion methods[10–12], we showed that damaging these regions indeed strongly a ects the functional network's communication e ciency and the balance between integration and segregation, which may lead to widespread cognitive de cits[13].

L Some of this type of lesion hubs having high WMD in the healthy connectome (the bilateral dACC, the bilateral paraCC, the le precentral gyrus and the le aMTG), while others have high nodal PC (the right IFG tri and IFG oper). e dACC, including the paraCC, monitors performance and signals the need for behavioral adaptation and is important to change behavior[45]. e le precentral gyrus is one of the primary motor regions and has been identi ed as a connector in a functional connectome[10]. e le aMTG belongs to the DMN and is a core region in the semantic system which bridges the memory based simulation system and the language-based semantic system[46]. e right IFG connects SSN, FPN and DMN, and has been shown to be a connector[12] that participates in a wide range of cognitive functions[42,43]. e right hippocampus has been identi ed as a connector[10] but does not show either high nodal PC or WMD in the current study.

Together we observed a complex correspondence between hubs in lesion models and those in the healthy system– e damages of the same type of hubs in the healthy connectome may cause the network topology to change towards di erent directions. is pattern is di erent from the simple correspondence (integrating e ect of connector "lesion" and segregating lesion e ect of provincial hub "lesion") revealed in some simulating lesion study[18], highlight the need to study the dynamic changes of functional networks upon brain damage. One potential mechanism is the connectional diaschisis[21,47,48]. Besides disconnections induced by the lesion, there may be a considerable number of increased functional connections that over-compensate for the brain damage to the functional connectome[49]. Future work is clearly desired to understand the di erent types of dynamics induced by lesion patterns encompassing di erent hub regions.

e dynamic changes of functional connection patterns among intact regions due to lesions elsewhere may also explain the existence of brain regions that showed high nodal WMD, gE or PC in the healthy connectome but did not have signi cant feature weights in the lesion models, including the posterior part of the DMN (e.g., PCC/PCu and lateral parietal cortex) and the right DLPFC. at is, although they are densely connected in the healthy network, their involvements in the brain lesion are not signi cantly predictive of the network topology.

ese results do not seem to be compromised by the fMRI data quality. All nodes except the le mPFC (a lesion

hub) satisfy the criteria for signal quality[50,51] (mean tSNR > 80, Fig. S11). Furthermore, these results are di cult to be explained by false negatives due to a lack of statistical power, because many of these regions have a decent proportion of cases of being damaged or preserved in our patient population (e.g., 19/96 patients were damaged in the right DLPFC; Fig. S1). We speculate that this phenomenon might be related to the following aspects. First, the brain is likely to be wired with su cient redundancy to increase resilience. Indeed, even a er severe brain injury, the network topology (e.g., small-worldness) is well preserved, although less optimal[52,53]. In simulation studies, attacking a small portion of critical regions induced limited impacts on network topology, with the network integrity sharply dropping only a er attacking 40% of degree-based hubs or 17% of connector hubs[10,54]. It is possible that the wiring redundancy is particularly pertinent to these regions, such that although they are normally well connected, routing possibilities for communication among other nodes are richer when they are no longer available because other regions are already connected. Another possibility is related to plasticity: when these regions are damaged, the rewiring among other regions is particularly e cient to compensate for the overall topological structure.

ere are several methodological issues to note. A common methodological issue in patient studies is that the lesion pattern is constrained by vascular properties, with some regions tending to be more prone to brain damage than others (Fig. S1), which results in power di erences among regions in some statistical testing. In contrast to univariate analysis, the method we employed, SVR, has no explicit assumptions regarding the nature of the data, such as the number of non-zero values in a feature vector, which is o en required by univariate correlation or t-test analyses. It is nonetheless worth noting that in many cases, a region's feature weight does not comply with the number of lesions: the FP orb (damaged in 4/96 patients), the le SFG (damaged in 3/96 patients), and the mPFC (damaged in 4/96 patients) were rarely damaged and yet were discovered to be lesion hubs. While multivariate approaches o er many advantages, the interpretation of individual feature requires caution. e feature weights, on which we relied to de ne hubs, were calculated in the context of the whole lesion patterns across patients. at is, it might be the complex patterns across the signi cant contributors that lead to the signi cant network changes. We thus chose to focus on those features that had signi cant weights as a group, considering them to have signi cant contributions to the functional network properties. e lack of simple characteristics of the hubs that were related to their segregating/integrating (local/global) role might be related to the multivariate information. Regarding the signs of feature weights, our univariate analyses using samples with single nodal lesion (the le insula) revealed topological changes in the same direction to that revealed by its sign in the SVR prediction model (integration e ect). Henson *et al.*[19] found that patients with focal hippocampus lesion also showed the same direction of results as our MVPA ndings (i.e., integration lesion e ect). ese two data points suggest the functional relevance of positive and negative weights in our current lesion models, although certainly convergent evidence is desired. A further important question is whether the mechanisms in which brain damage a ects functional network topology di ers across etiology. It has recently been shown that a wide range of brain disorders tend to implicate hub regions[17,55], the studies are far from conclusive auubs tlg thnn pt1(a)9.3000038(n)7.699, e999
oe vo vaug a1(n)2.9000001(a)-5.0990001(a)-5.099-etwor6(h)3.9000061(os)4.900

identical sequences of 3D T1 images were collected and averaged to improve the signal-to-noise ratio during analysis. Resting-state functional images along the AC–PC line were collected using the T2*-weighted echo planar image sequence with the following parameters: 28 axial slices, TR = 2000 ms, TE = 40 ms, FA = 90°, FOV = 210 mm × 210 mm, slice thickness = 4 mm, gap = 1 mm, duration = 4 min, and 120 volumes. During the resting-state scanning, participants were instructed to close their eyes, remain still, stay awake and not think about anything in particular. e FLAIR T2-weighted images, which had the same slice locations as the functional images on the axial plane, were collected with the following parameters: 28 slices, TR = 8002 ms, TE = 127.57 ms, TI = 2000 ms, FA = 90°, FOV = 250 mm × 250

$$Lp = \frac{N_{lesion\ \ voxles\ \ overlaped\ \ with\ \ the\ \ node}}{N_{voxel\ \ size\ \ of\ \ the\ \ node}} \quad (1)$$

SVRlesion model. *SVR lesion model*. We performed a linear SVR analysis with the default parameters (LIBSVM, http://www.csie.ntu.edu.tw/~cjlin/libsvm/) on each of the three network attributes. For a linear model, SVR can be described as

$$\mathrm{Y} = \omega^{T}\varphi(X) + b \quad (2)$$

where X is the lesion patterns across patients, Y is network attribute, $\varphi(X)$ is the function transforming the lesion patterns to a higher dimensional feature space, $\omega = (\omega_0, \omega_1, \omega_2, \quad)^{\mathrm{T}}$ is the tting coe cient (weight) in the high dimensional space, and b is the tting error.

Two nodes were not included because no patient had any lesion on them: the le occipital fusiform gyrus and the right temporal fusiform cortex.

e e ect of confounding factors. Some potential confounding variables, age, time a er lesion and total lesion volume, have been showed to be predictive for network topological metrics[52,65]. In this study, small but significant Pearson correlation coe cients were observed between total lesion volume and network locE ($r = 0.236$, $P = 0.021$) and gE ($r = 0.226$, $P = 0.027$), and between age and network locE ($r = -0.201$, $P = 0.049$) and sigma ($r = -0.263$, $P = 0.001$) (Table S2 and Fig. S12). No signi cant correlation was found between the network metrics and time a er lesion ($Ps > 0.17$; Table S2). However, the prediction weights of these two factors were not signi - cant in the SVR models.

Prediction accuracy and signi cance. In each turn of the LOOCV, one patient was designated as the test sample and the remaining patients were used to train the lesion model. e predicted score was then obtained by the feature matrix of the tested sample. A er all LOOCV rounds were completed, the Pearson correlation coe cients between the predicted and actual network attributes were computed to generate the predictive accuracy (Fig. 1).

Statistical signi cance of the predictive accuracy was determined using 1000 nonparametric permutation tests. For each permutation test, the prediction labels (i.e., the patients' network attributes) were randomized, and the same SVR prediction process as used in the actual data was carried out. A er 1000 permutations, a random distribution of accuracies was obtained and the P value was correspondingly calculated:

$$P = \frac{(\text{number of permutation accuracies} < \text{actual accuracy}) + 1}{\text{number of permutations} + 1} \quad (3)$$

L We de ned those features with signi cant weights, determined by permutation testing, as lesion hubs. e random distributions of feature weights were obtained according to the previous 1000 permutations. e signi cance of the feature weight was set at the < 2.5 or > 97.5 percentiles (i.e., $P < 0.05$ for a two-tailed test). For signi cant lesion models, regions with signi cant weights were mapped onto the cortical surfaces using the BrainNet Viewer package

13. Warren, D. E. *et al*. Network measures predict neuropsychological outcome a er brain injury. *Proceedings of the National Academy of Sciences of the United States of America* **111**, 14247–14252 (2014).
14. Guimera, R. & Nunes Amaral, L. A. Functional cartography of complex metabolic networks. *Nature* **433**, 895–900 (2005).
15. Mah, Y. H., Husain, M., Rees, G. & Nachev, P. Human brain lesion-de cit inference remapped. *Brain: a journal of neurology* **137**, 2522–2531 (2014).
16. Zhang, Y., Kimberg, D. Y., Coslett, H. B., Schwartz, M. F. & Wang, Z. Multivariate lesion-symptom mapping using support vector regression. *Hum Brain Mapp* **35**, 5861–5876 (2014).
17. Aerts, H., Fias, W., Caeyenberghs, K. & Marinazzo, D. Brain networks under attack: robustness properties and the impact of lesions. *Brain: a journal of neurology* **139**, 3063–3083 (2016).
18. Sporns, O., Honey, C. J. & Kotter, R. Identi cation and classi cation of hubs in brain networks. *PLoS One* **2**, e1049 (2007).
19. Henson, R. N. *et al*. e e ects of hippocampal lesions on MRI measures of structural and functional connectivity. *Hippocampus* **26**, 1447–1463 (2016).
20. Honey, C. J. & Sporns, O. Dynamical consequences of lesions in cortical networks. *Hum Brain Mapp* **29**, 802–809 (2008).
21. Alstott, J., Breakspear, M., Hagmann, P., Cammoun, L. & Sporns, O. Modeling the impact of lesions in the human brain. *PLoS Comput Biol* **5**, e1000408 (2009).
22. Smola, A. J. & Scholkopf, B. A tutorial on support vector regression. *Stat Comput* **14**, 199–222 (2004).
23. Dosenbach, N. U. *et al*. Prediction of individual brain maturity using fMRI. *Science* **329**, 1358–1361 (2010).
24. Chang, C. B. & Lin, C. J. LIBSVM: A Library for Support Vector Machines. *Acm T Intel Syst Tec* **2** (2011).
25. Craddock, R. B., James, G. A., Holtzheimer, P. E. 3rd, Hu, X. P. & Mayberg, H. S. A whole brain fMRI atlas generated via spatially constrained spectral clustering. *Hum Brain Mapp* **33**, 1914–1928 (2012).
26. Achard, S. & Bullmore, E. E ciency and cost of economical brain functional networks. *PLoS Comput Biol* **3**, e17 (2007).
27. Lin, Q. *et al*. A connectivity-based test-retest dataset of multi-modal magnetic resonance imaging in young healthy adults. *Sci Data* **2**, 150056 (2015).
28. Newman, M. E. Modularity and community structure in networks. *Proceedings of the National Academy of Sciences of the United States of America* **103**, 8577–8582 (2006).
29. Power, J. D., Plitt, M., Laumann, T. O. & Martin, A. Sources and implications of whole-brain fMRI signals in humans. *Neuroimage* **146**, 609–625 (2017).
30. Fan, L. *et al*. e Human Brainnetome Atlas: A New Brain Atlas Based on Connectional Architecture. *Cereb Cortex* **26**, 3508–3526 (2016).
31. Smith, D. V., Clithero, J. A., Rorden, C. & Karnath, H. O. Decoding the anatomical network of spatial attention. *Proceedings of the National Academy of Sciences of the United States of America* **110**, 1518–1523 (2013).
32. Pereira, F., Mitchell, T. & Botvinick, M. Machine learning classi ers and fMRI: a tutorial overview. *Neuroimage* **45**, S199–209 (2009).
33. Old eld, R. C. e assessment and analysis of handedness: the Edinburgh inventory. *Neuropsychologia* **9**, 97–113 (1971).
34. Achard, S. *et al*. Hubs of brain functional networks are radically reorganized in comatose patients. *Proceedings of the National Academy of Sciences of the United States of America* **109**, 20608–20613 (2012).
35. Crossley, N. A. *et al*. Cognitive relevance of the community structure of the human brain functional coactivation network. *Proceedings of the National Academy of Sciences of the United States of America* **110**, 11583–11588 (2013).
36. Vaishnavi, S. N. *et al*. Regional aerobic glycolysis in the human brain. *Proceedings of the National Academy of Sciences of the United States of America* **107**, 17757–17762 (2010).
37. Tomasi, D., Wang, G. J. & Volkow, N. D. Energetic cost of brain functional connectivity. *Proceedings of the National Academy of Sciences of the United States of America* **110**, 13642–13647 (2013).
38. Spetsieris, P. G. *et al*. Metabolic resting-state brain networks in health and disease. *Proceedings of the National Academy of Sciences of the United States of America* **112**, 2563–2568 (2015).
39. Xia, M. & He, Y. Magnetic resonance imaging and graph theoretical analysis of complex brain networks in neuropsychiatric disorders. *Brain connectivity* **1**, 349–365 (2011).
40. Fornito, A. & Bullmore, E. T. Connectomic intermediate phenotypes for psychiatric disorders. *Frontiers in psychiatry* **3**, 32 (2012).
41. Li, R. *et al*. Disrupted structural and functional rich club organization of the brain connectome in patients with generalized tonic-clonic seizure. *Hum Brain Mapp* **37**, 4487–4499 (2016).
42. Bertolero, M. A., Yeo, B. T. & D'Esposito, M. e modular and integrative functional architecture of the human brain. *Proceedings of the National Academy of Sciences of the United States of America* **112**, E6798–6807 (2015).
43. Yeo, B. T. *et al*. Functional Specialization and Flexibility in Human Association Cortex. *Cereb Cortex* **26**, 465 (2016).
44. Brass, M., Derrfuss, J., Forstmann, B. & von Cramon, D. Y. e role of the inferior frontal junction area in cognitive control. *Trends in Cognitive Sciences* **9**, 314–316 (2005).
45. Dosenbach, N. U. *et al*. Distinct brain networks for adaptive and stable task control in humans. *Proceedings of the National Academy of Sciences of the United States of America* **104**, 11073–11078 (2007).
46. Xu, Y., Lin, Q., Han, Z., He, Y. & Bi, Y. Intrinsic functional network architecture of human semantic processing: Modules and hubs. *Neuroimage* (2016).
47. Carrera, E. & Tononi, G. Diaschisis: past, present, future. *Brain: a journal of neurology* **137**, 2408–2422 (2014).
48. Fornito, A., Zalesky, A. & Breakspear, M. e connectomics of brain disorders. *Nature reviews. Neuroscience* **16**, 159–172 (2015).
49. Hillary, F. G. & Grafman, J. H. Injured Brains and Adaptive Networks: e Bene ts and Costs of Hyperconnectivity. *Trends Cogn Sci* **21**, 385–401 (2017).
50. Lo, C. Y. *et al*. Randomization and resilience of brain functional networks as systems-level endophenotypes of schizophrenia. *Proceedings of the National Academy of Sciences of the United States of America* **112**, 9123–9128 (2015).
51. Triantafyllou, C. *et al*. Comparison of physiological noise at 1.5 T, 3 T and 7 T and optimization of fMRI acquisition parameters. *Neuroimage* **26**, 243–250 (2005).
52. Nakamura, T., Hillary, F. G. & Biswal, B. B. Resting network plasticity following brain injury. *PLoS One* **4**, e8220 (2009).
53. Pandit, A. S. *et al*. Traumatic brain injury impairs small-world topology. *Neurology* **80**, 1826–1833 (2013).
54. Achard, S., Salvador, R., Whitcher, B., Suckling, J. & Bullmore, E. A resilient, low-frequency, small-world human brain functional network with highly connected association cortical hubs. *J Neurosci* **26**, 63–72 (2006).
55. Dai, Z. J., Bi, Y. C. & He, Y. With Great Brain Hub Connectivity Comes Great Vulnerability. *CNS neuroscience & therapeutics* **21**, 541–542 (2015).
56. Wang, J. *et al*. Disrupted functional brain connectome in individuals at risk for Alzheimer's disease. *Biological psychiatry* **73**, 472–481 (2013).
57. Skatun, K. C. *et al*. Consistent Functional Connectivity Alterations in Schizophrenia Spectrum Disorder: A Multisite Study. *Schizophr Bull* (2016).
58. Han, Z. *et al*. White matter structural connectivity underlying semantic processing: evidence from brain damaged patients. *Brain: a journal of neurology* **136**, 2952–2965 (2013).
59. Fang, Y. *et al*. e semantic anatomical network: Evidence from healthy and brain-damaged patient populations. *Hum Brain Mapp* **36**, 3499–3515 (2015).
60. Friston, K. J., Williams, S., Howard, R., Frackowiak, R. S. & Turner, R. Movement-related e ects in fMRI time-series. *Magn Reson Med* **35**, 346–355 (1996).

61. He, Y. *et al*